Micromechanical model for hydroxyapatite whisker reinforced polymer biocomposites

Weimin Yue and Ryan K. Roeder[a)]
Department of Aerospace and Mechanical Engineering, University of Notre Dame, Notre Dame, Indiana 46556

(Received 28 February 2006; accepted 5 June 2006)

A micromechanical model was developed to predict the elastic moduli of hydroxyapatite (HA) whisker reinforced polymer biocomposites based upon the elastic properties of each phase and the reinforcement volume fraction, morphology, and preferred orientation. The effects of the HA whisker volume fraction, morphology, and orientation distribution were investigated by comparing model predictions with experimentally measured elastic moduli for HA whisker reinforced high-density polyethylene composites. Predictions using experimental measurements of the HA whisker aspect ratio distribution and orientation distribution were also compared to common idealized assumptions. The best model predictions were obtained using the experimentally measured HA whisker aspect ratio distribution and orientation distribution.

I. INTRODUCTION

A. Hydroxyapatite-reinforced polymers

A variety of hydroxyapatite (HA), $Ca_{10}(PO_4)_6(OH)_2$, reinforced polymer composites have been investigated as orthopaedic biomaterials over the last two decades, including HA-reinforced polyethylene,[1–7] polyacrylics,[8–12] poly(α-hydroxy esters),[13–19] and polyetheretherketone,[20–25] among others. The rationale for HA-reinforced polymer composites is based on mimicking the mechanical and biological properties of bone tissue at the most fundamental hierarchical level. HA is the closest synthetic equivalent to human bone mineral, which is a calcium- and hydroxyl-deficient, carbonated apatite.[26,27] HA typically exhibits excellent biocompatibility, bioactivity, and, if porous, osteoconduction in vivo.[28–30] HA-reinforced polymer composites provide tailored mechanical properties that may be used to alleviate mechanical mismatch problems between bone tissue and synthetic bone substitutes or implants.

HA-reinforced high-density polyethylene (HDPE) was the first and most widely studied HA-reinforced polymer composite.[1–7] These composites have been commercialized under the trade name HAPEX, which has found clinical use in middle ear and maxillofacial implants.[5,31] The elastic modulus of HA-reinforced HDPE composites was isotropic and able to reach the lower regions of human cortical bone tissue as measured in the transverse direction (e.g., orthogonal to the longitudinal axis of long bones),[2,5] but remained short of the elastic modulus in the longitudinal direction and inadequate for load-bearing applications. Consequently, molecular orientation was introduced into the polymer to enhance the elastic modulus and mimic the anisotropy of bone tissue.[6] However, all the above studies cited for HA-reinforced polymers used an equiaxed HA powder, whereas the anisotropy in bone tissue is derived from the apatite crystals,[32,33] which have a platelike morphology elongated in the 002 crystallographic direction and oriented along directions of principal stress.[34–41]

HA whisker-reinforced polymer composites were recently developed to more accurately mimic the microstructure and mechanical properties of bone at the most fundamental hierarchical level.[40–42] The use of aligned HA whiskers instead of HA powder resulted in improved and anisotropic mechanical properties more similar to cortical bone tissue. HDPE reinforced with HA whiskers exhibited a significantly higher elastic modulus, ultimate tensile strength, and work to failure relative to composites reinforced with an equiaxed HA powder at equal volume fractions.[41] Mechanical anisotropy was introduced by a preferred orientation of HA whiskers in the polymer matrix, which increased the stiffness in the direction of the preferred orientation without sacrificing stiffness, relative to powder reinforcement, in the transverse direction. Thus, HA whisker-reinforced polymer composites are promising candidates for biomimetic synthetic bone substitutes and may also be used as a

[a)]Address all correspondence to this author.
e-mail: rroeder@nd.edu
DOI: 10.1557/JMR.2006.0263

model material for bone tissue at the most fundamental hierarchical level.

B. Micromechanical models for bone tissue

At the most fundamental hierarchical level, bone tissue is an apatite-reinforced collagen composite.[43] Micromechanical models for bone tissue have been based on this basic concept since the 1960s.[44,45] HA-reinforced polymer composites mimic bone tissue well at this level. Therefore, micromechanical models developed for bone tissue may also be applied to HA-reinforced polymer composites and vice versa.

In classic composites theory, a simple rule of mixtures is used to predict the effective mechanical behavior. An upper bound prediction was given by Voigt using an isostrain assumption,[46] and a lower bound prediction was given by Reuss using an isostress assumption.[47] Hashin–Shtrikman bounds provided a closer approximation allowing for an arbitrary phase geometry.[48] These simple models are unable to accurately predict the properties of bone tissue and other discontinuously reinforced composites that satisfy neither the isostrain nor isostress assumption.[49] Linear combinations of the Voigt and Reuss models, including Hill's model[50] and Hirsch's model,[51] have been used to more closely fit experimental data by introducing an empirical fitting factor. However, the fitting factors are material dependent, limiting general application of the model. Moreover, the above models consider only the volume fraction of each phase, which is inadequate for discontinuously reinforced composites.

Apatite crystals have an elongated, platelike morphology and exhibit preferred orientation along directions of principal stress.[34–41] Therefore, more recent micromechanical models sought to account for the reinforcement morphology and the arrangement of the reinforcement and matrix, in addition to the volume fraction of each phase.[52–54] For example, the Halpin–Tsai equations provide a complete and practical solution for a variety of reinforcement geometries (e.g., rod, plate, etc.) in terms of the reinforcement aspect ratio R (length/width).[55] Equations were derived from interpolations of exact solutions using Hill's "self consistent" models.[56] While the Halpin–Tsai equations account for the reinforcement morphology, reinforcements in a representative volume element (RVE) are assumed to be perfectly aligned, which is an unrealistic assumption in most discontinuously reinforced composites.

Tensor transformation laws were used to model the dependence of the elastic modulus of bone tissue on the misorientation angle θ between the axis of preferred orientation and the axis of applied stress.[45] Bundy proposed accounting for the orientation distribution of reinforcements in bone tissue by using a hypothetical orientation distribution function (ODF), $g(\theta)$, to describe the relative proportion of apatite crystals oriented in a solid angle between θ and $\theta + d\theta$.[57,58] Sasaki measured an ODF for apatite crystals in bone tissue using x-ray pole figure analysis and calculated the effective elastic moduli.[37,59] The 002 pole figures from three orthogonal sample faces were combined to calculate the ODF.[37] However, as noted by Wenk, the ODF determined by Sasaki was inaccurate because only a single 002 pole figure was measured.[39] ODFs were implemented for volume averaging elastic constants in polycrystalline materials by Bunge using Voigt, Reuss, or Hill assumptions.[60,61] In reinforced polymers, effective elastic constants have been calculated by volume averaging a RVE over an ODF using lamination theory[62] and aggregate averaging.[63–65] The reinforcement aspect ratio distribution has also been considered in numerical models using the latter approach.[66,67]

The objective of this study was to develop a micromechanical model to predict biocomposite elastic properties using only measurable microstructural parameters. The effects of the HA reinforcement volume fraction, morphology, and orientation distribution were investigated by comparing model predictions with experimentally measured elastic moduli for HA whisker-reinforced HDPE composites. Predictions using experimental measurements of the HA whisker aspect ratio distribution and orientation distribution were also compared to common idealized assumptions.

II. MATERIALS AND METHODS

A. Biocomposite processing and mechanical characterization

HA-reinforced HDPE biocomposites were processed and characterized for up to 50 vol% HA whiskers or powder as described in a previous paper.[41] Briefly, single-crystal HA whisker reinforcements were hydrothermally synthesized at low temperature ($\leqslant$200 °C) from chemical solutions containing calcium, phosphate, and a calcium chelating agent.[68] A commercially available equiaxed HA powder (Product No. 21221, Fluka Chemical Corp., Milwaukee, WI) was used to produce composites with randomly oriented HA reinforcements for normalization of the texture measurements for HA whisker reinforced composites. HDPE polymer powder was produced from commercially available HDPE polymer beads (Product No. 427977, Aldrich Chemical Co., Inc., Milwaukee, WI). HA and HDPE powders were ultrasonically co-dispersed in ethanol with a sonic dismembrator. Composite powder mixtures were vacuum filtered, dried, and densified by uniaxial pressing at ambient temperature with a cylindrical pellet die. The dense composite preforms were then placed in the center of a channel die and heated above the polymer melting point to 145 °C. Upon compression molding, the viscous

reinforced polymer was extruded bilaterally toward the open ends of the mold, and HA whisker reinforcements were aligned along the length of the bar. The longitudinal elastic modulus E and other mechanical properties were measured in uniaxial tension using standard machined specimens (ASTM D 638-01, Type V).[69]

B. Microstructural characterization

In the previous study, the size and aspect ratio distribution were measured for the as-synthesized HA whiskers.[41] The preferred orientation of HA whiskers in composites was qualitatively characterized using conventional powder x-ray diffraction (XRD) on polished sections for each of the three orthogonal specimen directions. In this study, the size, aspect ratio, and orientation distribution of HA whiskers were each quantitatively measured after composite processing.

1. Reinforcement morphology

The size and aspect ratio of HA whiskers in composites after compression molding were characterized using quantitative stereology. Composites were heated to 600 °C to pyrolyze the HDPE matrix without affecting the HA whisker morphology. Microscopy slides were prepared by ultrasonically dispersing 0.003 g of the residual HA whiskers in 1 ml methanol and pipetting drops of the suspension onto a glass slide placed in an oven at 90 °C to quickly evaporate the methanol. Measurements of whisker length and width were taken using an optical microscope (Eclipse ME600L, Nikon Instruments, Inc., Melville, NJ) and a digital camera (Magnafire, Olympus America, Melville, NJ) connected to a personal computer with image analysis software (Object-Image 2.08, NIH Image). All slides were analyzed at 400× magnification. A 10 × 10 square grid was digitally overlaid using the image analysis software to facilitate random whisker selection at grid nodes. The aspect ratio R was calculated by dividing the whisker length by the width. A total of 500 whiskers were measured in this manner for composites varying from 10 to 50 vol% HA whiskers. Analysis of variance (ANOVA; Statview 5.01, SAS Institute, Inc., Cary, NC) was used to compare groups. Post-hoc comparisons were performed using a Student's T-test. A log transform of the aspect ratio data was used to provide a normal distribution for statistical analysis.

2. Texture analysis

Quantitative measurement of the preferred orientation of HA whiskers in composites was performed using a General Area Detector Diffraction System (GADDS) equipped with a two-dimensional HI-STAR detector (Bruker AXS Inc., Madison, WI). Specimens were sectioned from the center of tensile bars using a low-speed diamond wafer saw, and the surface orthogonal to the longitudinal specimen direction was polished using a series of diamond compounds and aluminum oxide to a 0.05 μm final polish. Polished specimens were mounted on the goniometer and aligned using a laser-video microscope. Monochromatic Cu K_α radiation was generated at 40 kV and 40 mA and focused on the specimen by a 0.5 mm diameter pinhole collimator. The distance between the specimen surface and detector was set to 120 mm.

Two-dimensional diffraction patterns were collected for HA whisker-reinforced HDPE composites at each reinforcement volume fraction. The 002, 200, and 222 reflections for HA were chosen due to relatively sharp distinction and their relationship to the crystal habit of HA whiskers (Fig. 1). Pole figures for the 002, 200, and 222 reflections were obtained by two methods. First, composite specimens were rotated about the longitudinal specimen axis in 5° increments, and a total of 72 diffraction patterns were obtained over the orientation space ($0° < \theta < 360°$). The diffraction patterns were integrated using the GADDS software to determine the pole figure. This method made no assumptions regarding the symmetry of the HA whisker orientation distribution but required a significantly longer time for data collection. However, results from this method showed an axisymmetric HA whisker orientation distribution. Therefore, a second method was used to dramatically reduce the time required for data collection by assuming an axisymmetric HA whisker orientation distribution. Composite specimens mounted on the goniometer were continuously rotated about the same longitudinal specimen axis and the obtained diffraction pattern was processed by GADDs software to determine the pole figures. Pole figure data was corrected by eliminating background intensity differences using untextured reference pole figures for composites reinforced with equal volume fractions of the

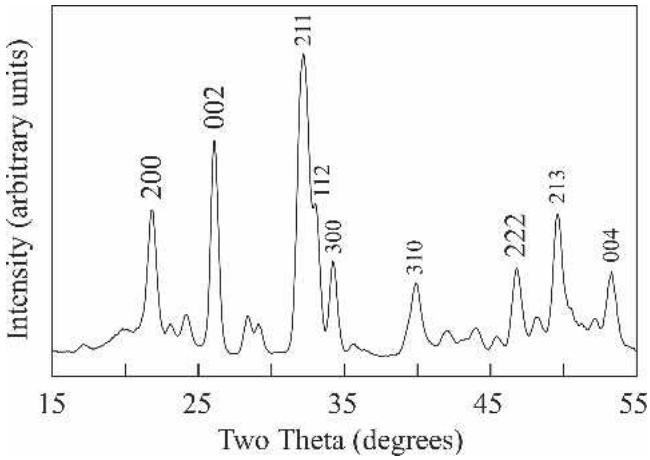

FIG. 1. Representative XRD pattern collected by GADDS for a 30 vol% HA whisker-reinforced HDPE composite showing prominent reflections for HA, including the 200, 002, and 222 reflections, which were used for texture analysis.

equiaxed HA powder. The three corrected pole figures for the 002, 200, and 222 reflections were combined and the orientation distribution function (ODF) was calculated using the Arbitrarily Defined Cells (ADC) method (LaboTex, Version 2.1, LaboSoft s.c., Krakow, Poland). Finally, the preferred orientation was quantified in multiples of a random distribution (MRD), which were calculated by averaging and normalizing ODFs at 5° intervals from the longitudinal specimen axis.

C. Micromechanical model

A micromechanical model was developed for discontinuously reinforced composites, such as bone tissue or HA whisker-reinforced polymers. The elastic modulus of a representative volume element (RVE) $E(R,\theta)$, composed of a matrix material with reinforcements of fixed aspect ratio R and fixed orientation angle θ to the loading direction, was calculated by combining Halpin–Tsai equations[55] and tensor transformation laws. Note, however, that the properties of the RVE could also be calculated using other similar models (e.g., Mori–Tanaka) or finite element analysis. RVEs of varying reinforcement aspect ratio and orientation angle were averaged using the experimentally measured reinforcement aspect ratio distribution function $f(R)$ and ODF $g(\theta)$ (Fig. 2). Thus, the effective elastic modulus for a given loading direction was calculated as

$$\bar{E} = \frac{\int_\theta \int_R g(\theta)\cdot f(R)\cdot E(R,\,\theta)\cdot dR\cdot d\theta}{\int_\theta \int_R g(\theta)\cdot f(R)\cdot dR\cdot d\theta} \quad , \qquad (1)$$

where

$$E(R,\,\theta) = \left[\frac{\cos^4(\theta)}{E_L} + \frac{\sin^4(\theta)}{E_T} + \sin^2(\theta)\cdot\cos^2(\theta) \cdot\left(\frac{1}{G_{LT}} - \frac{2\cdot\nu_{LT}}{E_L}\right)\right]^{-1} \quad . \qquad (2)$$

In Eq. (2), E_L, E_T, G_{LT}, and ν_{LT} are the elastic moduli and Poisson's ratio of the RVE calculated using the following Halpin–Tsai equations:

$$E_L = E_m\cdot\frac{1 + a_L\cdot\eta_L\cdot V_r}{1 - \eta_L\cdot V_r} \quad ,$$

$$\eta_L = \frac{\frac{E_{33}}{E_m} - 1}{\frac{E_{33}}{E_m} + a_L} \quad ,$$

$$a_L = 2\cdot R + 40\cdot V_r^{10} \quad , \qquad (3)$$

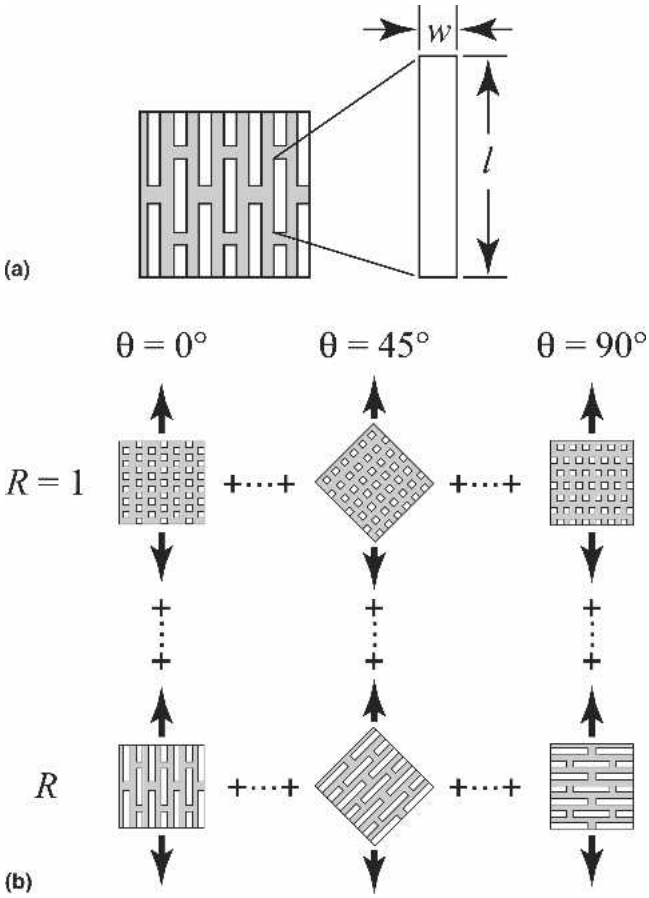

FIG. 2. Schematic diagram of the micromechanical model showing (a) the representative volume element (RVE) with reinforcements of fixed aspect ratio ($R = l/w$) and (b) averaging of all RVEs with varying reinforcement aspect ratio and misorientation.

$$E_T = E_m\cdot\frac{1 + a_T\cdot\eta_T\cdot V_r}{1 - \eta_T\cdot V_r} \quad ,$$

$$\eta_T = \frac{\frac{E_{11}}{E_m} - 1}{\frac{E_{11}}{E_m} + a_T} \quad ,$$

$$a_T = 2 + 40\cdot V_r^{10} \quad , \qquad (4)$$

$$G_{LT} = G_m\cdot\frac{1 + a_{LT}\eta_{LT}\cdot V_r}{1 - \eta_{LT}\cdot V_r} \quad ,$$

$$\eta_{LT} = \frac{\frac{G_{44}}{G_m} - 1}{\frac{G_{44}}{G_m} + a_{LT}} \quad ,$$

$$a_{LT} = 1 + 40\cdot V_r^{10} \quad , \qquad (5)$$

$$\nu_{LT} = \nu_{13}\cdot V_r + \nu_m\cdot(1 - V_r) \quad , \qquad (6)$$

where R is the reinforcement aspect ratio and V_r is the reinforcement volume fraction.

The elastic modulus of the HDPE polymer matrix E_m was measured in uniaxial tension with standard specimens (ASTM D 638-01, Type V, $n = 5$)[69] machined after compressing molding using the methods described above. The elastic modulus for HDPE in the longitudinal specimen direction was 1.3 ± 0.1 GPa (mean ± standard deviation). The HDPE matrix was determined to be nearly isotropic from stiffness coefficients measured using ultrasonic wave propagation. Therefore, the shear modulus G_m was calculated as

$$G_m = \frac{E_m}{2\cdot(1 + \nu_m)} \quad , \tag{7}$$

where Poisson's ratio, ν_m was taken as 0.35.[70] Measured stiffness coefficients for HA were taken from the literature[71] in order to calculate the elastic moduli and Poisson's ratio as $E_{11} = 114$ GPa, $E_{33} = 138$ GPa, $G_{44} = 40$ GPa, and $\nu_{13} = 0.31$, respectively. Finally, for comparison, upper and lower bound predictions were also calculated using classic composites theory with the assumption of isostrain and isostress, respectively.

III. RESULTS

A. Reinforcement morphology

The mean aspect ratio measured for the as-synthesized whiskers and 10–50 vol% of the same whiskers in HDPE composites after processing is shown in Fig. 3. The as-synthesized whiskers had a mean aspect ratio of approximately 8. After composite processing, the mean whisker aspect ratio decreased to approximately 4 and to nearly 2 in composites reinforced with 10–40 vol% and 50 vol% HA whiskers, respectively. Statistically significant differences ($p < 0.0001$) existed between the as-synthesized HA whiskers, composites with 10–40 vol% HA whiskers, and composites with 50 vol% HA whiskers. There were no statistically significant differences between composites containing 10–40 vol% whiskers ($p > 0.05$).

B. Texture analysis

The preferred orientation of HA whiskers in composites was quantified by ODFs calculated from pole figures. ODFs were plotted on inverse pole figures showing the orthogonal specimen axes mapped on the crystallographic orientation space (Fig. 4). Pole figures recalculated from the ODFs showed the crystallographic axes mapped on the specimen orientation space (Fig. 5). To compare composites reinforced with different volume fractions of HA whiskers, ODFs were normalized using multiples of a random distribution (MRD), such that ODFs for each volume fraction had the same integrated area (Fig. 6). The degree of preferred orientation along the longitudinal specimen axis ($\theta = 0°$) was 2.5, 2.4, 2.4, 1.8, and 1.4 MRD for 10, 20, 30, 40, and 50 vol% HA whiskers, respectively (Fig. 6). Note that a MRD value of unity corresponds to a random distribution. Thus, all composites exhibited a crystallographic and morphological preferred orientation of the single-crystal HA whiskers in the longitudinal specimen axis, and the degree of preferred orientation decreased for increased HA volume fraction in composites (Fig. 6).

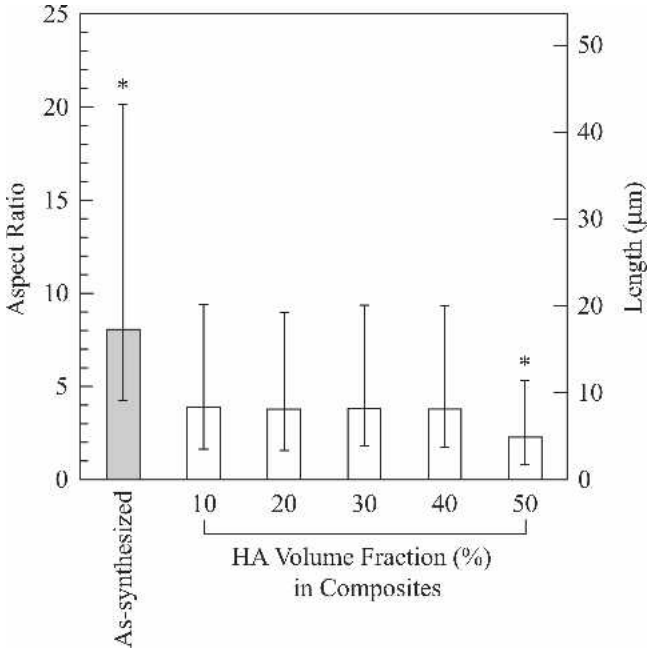

FIG. 3. Mean aspect ratio measured for the as-synthesized HA whiskers and 10–50 vol% of the same whiskers in composites after processing, showing whisker degradation. Note that the whisker width for each group was nearly constant permitting the whisker length to be shown on the secondary y axis. Error bars span the first standard deviation. Asterisks (*) denote a statistically significant difference ($p < 0.0001$) with all other groups.

C. Micromechanical model

Micromechanical model predictions for the longitudinal composite elastic modulus $\bar{E}$ were compared to experimental measurements from a previous study.[41] The effects of the HA whisker reinforcement volume fraction, morphology, and preferred orientation were investigated

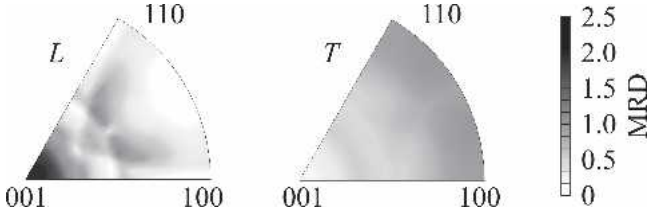

FIG. 4. Inverse pole figures calculated for HDPE reinforced with 30 vol% HA whiskers, showing the longitudinal (L) and transverse (T) specimen axes plotted in the crystallographic space shown. The orientation distribution is shown in units of MRD.

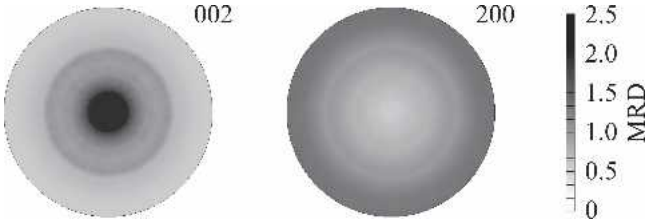

FIG. 5. Pole figures recalculated from ODFs for HDPE reinforced with 30 vol% HA whiskers, showing the 002 and 200 crystallographic axes plotted on a stereographic projection of the specimen orientation space defined by the longitudinal (coming out of the paper) and transverse (in the plane of the paper) axes. The orientation distribution is shown in units of MRD.

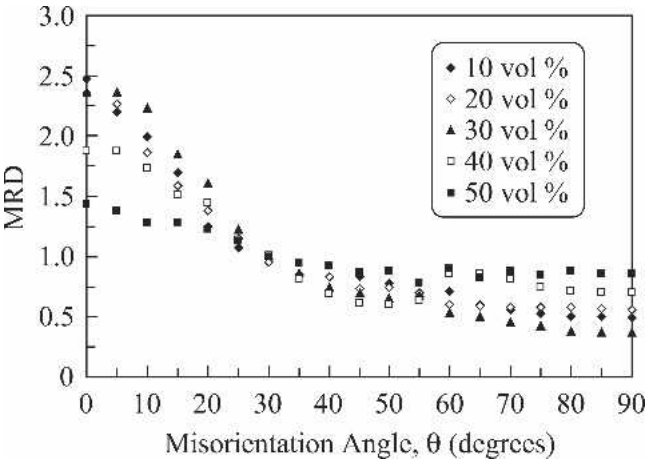

FIG. 6. Axisymmetric orientation distribution functions (ODFs) measured for HDPE composites reinforced with 10 to 50 vol% HA whiskers. The degree of preferred orientation is shown in MRD.

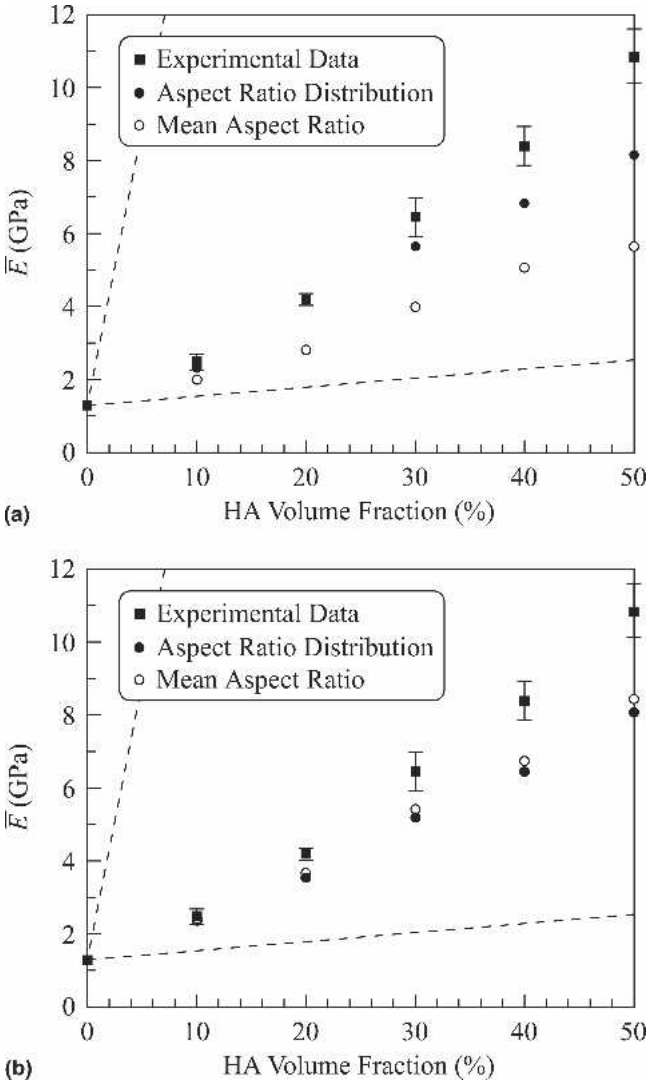

FIG. 7. Longitudinal composite elastic modulus $\bar{E}$ as a function of HA whisker volume fraction, showing (■) experimentally measured data compared to micromechanical model predictions using the experimentally measured whisker ODF and either the (●) aspect ratio distribution or (○) mean aspect ratio for (a) whiskers in composites or (b) as-synthesized whiskers. Error bars for experimental data span the first standard deviation. Upper and lower bound predictions are shown by dashed lines for comparison.

in the micromechanical model. Predictions using experimental measurements of the HA whisker aspect ratio and orientation distribution were compared to common idealized assumptions.

The longitudinal composite elastic modulus was calculated as a function of the HA whisker volume fraction using the measured whisker ODF and either the mean aspect ratio or aspect ratio distribution of whisker reinforcements measured for each HA volume fraction in composites [Fig. 7(a)]. Predictions using the measured whisker aspect ratio distribution were much closer to the experimental data than predictions using the mean aspect ratio for each HA volume fraction. The model prediction using the measured whisker aspect ratio distribution provided a good approximation of the experimentally measured data, except when the HA volume fraction was greater than 30 vol%, with increasing underestimation from 30–50 vol%.

The effects of whisker degradation during processing were examined by comparing model predictions using the measured aspect ratio distribution for the as-synthesized HA whiskers [Fig. 7(b)] versus that for the whiskers in composites after processing [Fig. 7(a)]. Predictions using the aspect ratio distribution after processing [Fig. 7(a)] were similar to predictions using the aspect ratio distribution from the as-synthesized whiskers [Fig. 7(b)]. The difference between predictions for the mean aspect ratio and the aspect ratio distribution was much less for the as-synthesized HA whiskers [Fig. 7(b)] compared to whiskers in composites after processing [Fig. 7(a)].

The effects of the HA whisker preferred orientation on the micromechanical model predictions are shown in Fig. 8. The idealized assumptions of perfectly aligned or

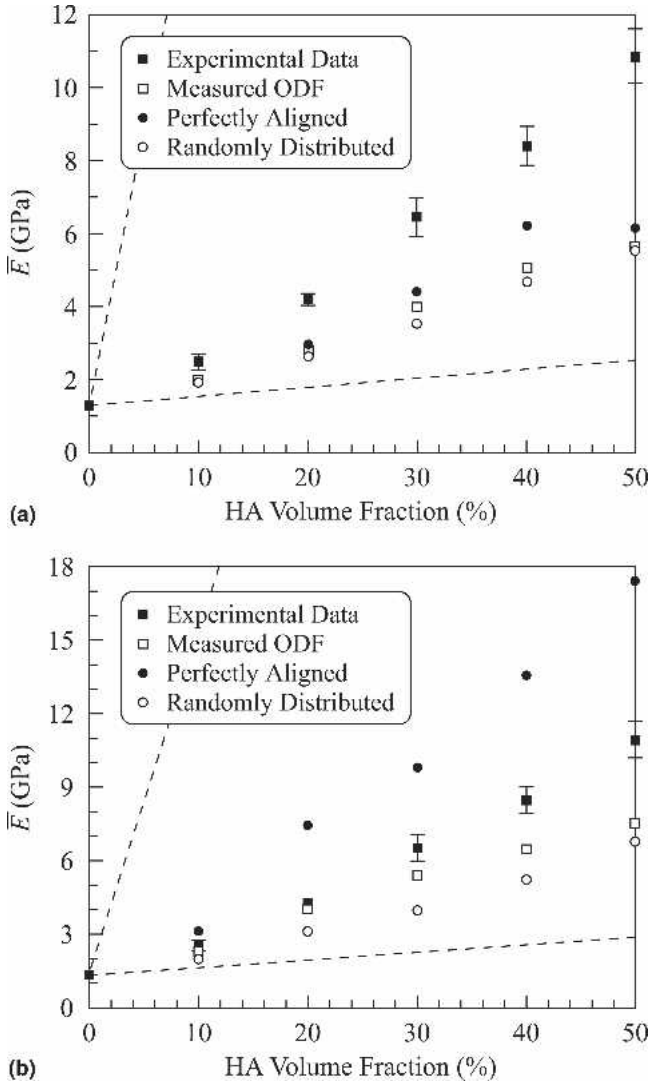

FIG. 8. The longitudinal composite elastic modulus $\bar{E}$ as a function of HA whisker volume fraction, showing (■) experimentally measured data compared to micromechanical model predictions using the (□) experimentally measured, (●) perfectly aligned, or (○) randomly distributed whisker ODF, and either the experimentally measured (a) mean aspect ratio or (b) aspect ratio distribution for whisker reinforcements. Error bars for experimental data span the first standard deviation. Upper and lower bound predictions are shown by dashed lines for comparison.

randomly distributed HA whiskers in composites were compared to the experimentally measured HA whisker ODF in composites. Additionally, the mean aspect ratio [Fig. 8(a)] and aspect ratio distribution [Fig. 8(b)] for HA whiskers in composites were examined separately. Using either the mean aspect ratio [Fig. 8(a)] or aspect ratio distribution [Fig. 8(b)] of HA whiskers in composites, perfectly aligned HA whiskers provided the highest estimation while randomly distributed HA whiskers provided the lowest estimation, as expected. Predictions using the experimentally measured ODF in the model were located in between the extreme assumptions, also as expected. All predictions using the measured mean aspect ratio of HA whiskers underestimated the experimental data [Fig. 8(a)]. On the other hand, the HA whisker aspect ratio distribution provided a more reasonable prediction [Fig. 8(b)]. The assumptions of perfectly aligned and randomly oriented whiskers in the model over- and underestimated, respectively, the measured longitudinal composite elastic modulus [Fig. 8(b)]. The measured ODF for composites provided the closest match to the experimental data [Fig. 8(b)]. In summary, the micromechanical model provided the best estimation of the experimentally measured composite elastic modulus using the measured aspect ratio distribution and ODF for HA whiskers in composites.

IV. DISCUSSION

The results of this study demonstrate the benefits of using statistical distributions (or distribution functions) for microstructural parameters in micromechanical models. The micromechanical model in this study accounted for the elastic properties of each phase, and the HA whisker volume fraction, aspect ratio distribution, and orientation distribution. All predictions using this model were substantially better than the classical upper and lower bound predictions. More importantly, the measured HA whisker aspect ratio and orientation distributions enabled the micromechanical model to more realistically account for the physical arrangement of HA whisker reinforcements in the polymer matrix. Without this approach, predictions using the Halpin–Tsai equations would consider only the reinforcement morphology and would be the same as using the perfectly aligned ODF and mean aspect ratio [Fig. 8(a)]. Model predictions using both the measured ODF and aspect ratio distribution provided the best approximation of the experimentally measured elastic modulus [Fig. 8(b)].

Micromechanical model predictions were quite sensitive to both the ODF and aspect ratio distribution. Predictions using the measured ODF and idealized assumptions of perfectly aligned or randomly oriented whiskers exhibited substantial variation within the upper and lower bounds [Fig. 8(b)]. The difference between predictions using the measured ODF and the assumption of randomly oriented whiskers (MRD = 1) was particularly noteworthy, considering that similar to bone, the composites of this study exhibited a relatively weak texture (MRD ≈ 2) compared to the theoretical possibilities ($0 < \text{MRD} < \infty$). Predictions using the aspect ratio distribution were also substantially different from those using the mean aspect ratio [Fig. 7(a)]. Furthermore, predictions comparing the measured ODF to idealized assumptions exhibited much less variation when the mean aspect ratio was used [Fig. 8(a)] than when the aspect

ratio distribution was used [Fig. 8(b)]. One reason for this effect was that the measured whisker aspect ratio distributions were log normal (Fig. 3). Thus, model predictions were most sensitive to the high aspect ratio portion of the distribution, even though these whiskers composed a relatively small fraction of the total.

Another interesting result is that whisker degradation during processing may not affect the composite elastic properties as much as is typically expected. Model predictions using the aspect ratio distribution of as-synthesized whiskers and whiskers in composites after processing were similar, while predictions using the mean whisker aspect ratio showed a large difference (Fig. 7). Recall that the mean HA whisker aspect ratio decreased after processing; however, the aspect ratio distribution showed that relatively large whiskers remained in the HDPE matrix (Fig. 3). The aspect ratio distribution for both the as-synthesized whiskers and whiskers in composites was log normal. Therefore, the results demonstrate that a relatively small volume of high aspect ratio whiskers can contribute disproportionately to the effective elastic properties.

Micromechanical model predictions were based on measured data for important microstructural features and provided a good approximation of experimentally measured elastic moduli. However, even the best model predictions still deviated from the experimentally measured properties at high whisker volume fractions [e.g., Fig. 8(b)]. Several factors could account for this discrepancy. The most likely cause is the increasing likelihood of whisker–whisker interactions at high volume fractions. The assumption of perfectly distributed reinforcements in the model's RVE ignores this effect. Molecular orientation in the HDPE polymer matrix may have occurred due to shear flow during compression molding.[4] In this case, the molecular preferred orientation would coincide with the loading direction and might also contribute to the elastic anisotropy. However, this factor is considered unlikely in this study because HDPE processed without HA reinforcements was measured to have nearly isotropic stiffness coefficients and the model error increased with increasing whisker volume fraction.

The micromechanical model investigated in this study could also be used to model the mineralized extracellular matrix of bone tissue as an apatite-reinforced collagen composite or as part of a multiscale model for the hierarchical structure of bone. Apatite crystals in bone tissue are elongated and have a preferred orientation along directions of principal stress (e.g., the longitudinal axis of long bones).[34–41] Thus, measurements of the apatite crystal aspect ratio distribution and orientation distribution could be used in this micromechanical model to improve predictions for the mechanical properties of bone tissue.

V. CONCLUSIONS

A micromechanical model was developed to predict the elastic moduli of HA whisker-reinforced polymer biocomposites based upon the elastic properties of each phase and the reinforcement volume fraction, morphology, and preferred orientation. Model predictions using an experimentally measured HA whisker aspect ratio distribution and ODF provided the best approximation of the experimentally measured elastic modulus. Common idealized microstructural assumptions, such as a mean aspect ratio and perfectly or randomly oriented whiskers, were shown to result in substantial inaccuracies.

ACKNOWLEDGMENTS

This research was partially supported by the Indiana 21st Century Research and Technology Fund and the National Institutes of Health (AR049598). The authors thank Keith J. Bowman and Jacob Jones at Purdue University for providing training and use of the GADDS. The authors also thank Robert J. Kane for preparation of HDPE specimens for mechanical testing.

REFERENCES

1. W. Bonfield, M.D. Grynpas, A.E. Tully, J. Bowman, and J. Abram: Hydroxyapatite reinforced polyethylene—A mechanically compatible implant material for bone-replacement. *Biomaterials* **2,** 185 (1981).
2. W. Bonfield: Composites for bone replacement. *J. Biomed. Eng.* **10,** 522 (1988).
3. W. Bonfield, J.A. Bowman and M.D. Grynpas: Composite material for use in orthopaedics, U.S. Patent No. 5 017 627 (1991).
4. N.H. Ladizesky, I.M. Ward, and W. Bonfield: Hydroxyapatite/high-performance polyethylene fibre composites for high-load-bearing bone replacement materials. *J. Appl. Polym. Sci.* **65,** 1865 (1997).
5. M. Wang, R. Joseph, and W. Bonfield: Hydroxyapatite-polyethylene composites for bone substitution: Effects of ceramic particle size and morphology. *Biomaterials* **19,** 2357 (1998).
6. M. Bonner, L.S. Saunders, I.M. Ward, G.W. Davies, M. Wang, K.E. Tanner, and W. Bonfield: Anisotropic mechanical properties of oriented HAPEX^{TM}. *J. Mater. Sci.* **37,** 325 (2002).
7. L. Di Silvio, M.J. Dalby, and W. Bonfield: Osteoblast behaviour on HAP/PE composite surfaces with different HA volumes. *Biomaterials* **23,** 101 (2002).
8. E.J. Harper, J.C. Behiri, and W. Bonfield: Flexural and fatigue properties of a bone cement based upon polyethylmethacrylate and hydroxyapatite. *J. Mater. Sci.: Mater. Med.* **6,** 799 (1995).
9. K.E. Watson, K.S. Tenhuisen, and P.W. Brown: The formation of hydroxyapatite-calcium polyacrylate composites. *J. Mater. Sci.: Mater. Med.* **10,** 205 (1999).
10. Y.E. Greish and P.W. Brown: An evaluation of mechanical property and microstructural development in HAp-Ca polycarboxylate biocomposites prepared by hot pressing. *J. Biomed. Mater. Res. Appl. Biomater.* **53,** 421 (2000).
11. M. Kobayashi, T. Nakamura, Y. Okada, A. Fukumoto, T. Furukawa, H. Kato, T. Kokobu, and T. Kikutani: Bioactive bone cement: Comparison of apatite and wollastonite containing glass-ceramic,

hydroxyapatite, and β-tricalcium phosphate fillers on bone bonding strength. *J. Biomed. Mater. Res.* **42,** 223 (1998).
12. S. Shinzato, M. Kobayashi, W.F. Mousa, M. Kamimura, M. Neo, Y. Kitamura, T. Kokubo, and T. Nakamura: Bioactive polymethyl methacrylate-based bone cement: Comparison of glass beads, apatite- and wollastonite-containing glass-ceramic, and hydroxyapatite fillers on mechanical and biological properties. *J. Biomed. Mater. Res.* **51,** 258 (2000).
13. S. Higashi, T. Yamamura, T. Nakamura, Y. Ikada, S-H. Hyon, and K. Jamshidi: Polymer-hydroxyapatite composites for biodegradable bone fillers. *Biomaterials* **7,** 183 (1986).
14. C.C.P.M. Verheyen, J.R. de Wijn, C.A. van Blitterswijk, and K. de Groot: Evaluation of hydroxylapatite/poly(L-lactide) composites: Mechanical behavior. *J. Biomed. Mater. Res.* **26,** 1277 (1992).
15. M. Kikuchi, Y. Suetsugu, J. Tanaka, and M. Akao: Preparation and mechanical properties of calcium phosphate/copoly-L-lactide composites. *J. Mater. Sci.: Mater. Med.* **8,** 361 (1997).
16. N. Ignjatovic, S. Tomic, M. Dakic, M. Miljkovic, M. Plavsic, and D. Uskokovic: Synthesis and properties of hydroxyapatite/poly-L-lactide composite biomaterials. *Biomaterials* **20,** 809 (1999).
17. Y. Shikinami and M. Okuno: Bioresorbable devices made of forged composites of hydroxyapatite (HA) particles and poly-L-lactide (PLLA): Part I. Basic characteristics. *Biomaterials* **20,** 859 (1999).
18. C. Durucan and P.W. Brown: Low temperature formation of calcium-deficient hydroxyapatite-PLA/PLGA composites. *J. Biomed. Mater. Res.* **51,** 717 (2000).
19. C. Durucan and P.W. Brown: Calcium-deficient hydroxyapatite-PLGA composites: Mechanical properties and microstructural characterization. *J. Biomed. Mater. Res.* **51,** 726 (2000).
20. M.S. Abu Bakar, P. Cheang, and K.A. Khor: Thermal processing of hydroxyapatite reinforced polyetheretherketone composites. *J. Mater. Process. Technol.* **89–90,** 462 (1999).
21. M.S. Abu Bakar, P. Cheang, and K.A. Khor: Mechanical properties of injection molded hydroxyapatite-polyetheretherketone biocomposites. *Compos. Sci. Technol.* **63,** 421 (2003).
22. M.S. Abu Bakar, P. Cheang, and K.A. Khor: Tensile properties and microstructural analysis of spheroidized hydroxyapatite-poly (etheretherketone) biocomposites. *Mater. Sci. Eng., A* **345,** 55 (2003).
23. M.S. Abu Bakar, M.H.W. Cheng, S.M. Tang, S.C. Yu, K. Liao, C.T. Tan, K.A. Khor, and P. Cheang: Tensile properties, tension-tension fatigue and biological response of polyetheretherketone-hydroxyapatite composites for load-bearing orthopedic implants. *Biomaterials* **24,** 2245 (2003).
24. M. Wang: Developing bioactive composite materials for tissue replacement. *Biomaterials* **24,** 2133 (2003).
25. S.M. Tang, P. Cheang, M.S. Abu Bakar, K.A. Khor, and K. Liao: Tension-tension fatigue behavior of hydroxyapatite reinforced polyetheretherketone composites. *Int. J. Fatigue* **26,** 49 (2004).
26. L.L. Hench: Bioceramics: From concept to clinic. *J. Am. Ceram. Soc.* **74,** 1487 (1991).
27. R.Z. LeGeros and J.P. LeGeros: Dense hydroxyapatite, in *An Introduction to Bioceramics*, edited by L.L. Hench and J. Wilson (World Scientific Publishing Co., NJ, 1993), pp. 139–180.
28. L.L. Hench: Bioceramics. *J. Am. Ceram. Soc.* **81,** 1705 (1998).
29. R. Holmes, V. Mooney, R. Bucholz, and A. Tencer: A coralline hydroxyapatite bone graft substitute. *Clin. Orthop. Relat. Res.* **188,** 252 (1984).
30. H. Oguchi, K. Ishikawa, K. Mizoue, K. Seto, and G. Eguchi: Long-term histological evaluation of hydroxyapatite ceramics in humans. *Biomaterials* **16,** 33 (1995).
31. J.L. Dornhoffer: Hearing results with the Dornhoffer ossicular replacement prostheses. *Laryngoscope* **108,** 531 (1998).
32. K. Hasegawa, C.H. Turner, and D.B. Burr: Contribution of collagen and mineral to the elastic anisotropy of bone. *Calcif. Tissue Int.* **55,** 381 (1994).
33. Y. Takano, C.H. Turner, and D.B. Burr: Mineral anisotropy in mineralized tissues is similar among species and mineral growth occurs independently of collagen orientation in rats: Results from acoustic velocity measurements. *J. Bone Miner. Res.* **11,** 1292 (1996).
34. S. Weiner and P.A. Price: Disaggregation of bone into crystals. *Calcif. Tissue Int.* **39,** 365 (1986).
35. S. Weiner and W. Traub: Bone structure: From angstroms to microns. *FASEB J.* **6,** 879 (1992).
36. G.E. Bacon, P.J. Bacon, and R.K. Griffiths: Study of bones by neutron-diffraction. *J. Appl. Crystallogr.* **10,** 124 (1977).
37. N. Sasaki, N. Matsushima, N. Ikawa, H. Yamamura, and A. Fukuda: Orientation of bone mineral and its role in the anisotropic mechanical properties of bone–Transverse anisotropy. *J. Biomech.* **22,** 157 (1989).
38. N. Sasaki and Y. Sudoh: X-ray pole figure analysis of apatite crystals and collagen molecules in bone. *Calcif. Tissue Int.* **60,** 361 (1997).
39. H.R. Wenk and F. Heidelbach: Crystal alignment of carbonated apatite in bone and calcified tendon: Results from quantitative texture analysis. *Bone* **24,** 361 (1999).
40. R.K. Roeder, M.M. Sproul, and C.H. Turner: Hydroxyapatite whisker reinforcements used to produce anisotropic biomaterials. *Trans. Orthop. Res. Soc.* **26,** 528 (2001).
41. R.K. Roeder, M.M. Sproul, and C.H. Turner: Hydroxyapatite whiskers provide improved mechanical properties in reinforced polymer composites. *J. Biomed. Mater. Res.* **67A,** 801 (2003).
42. G.L. Converse and R.K. Roeder: Tensile properties of hydroxyapatite whisker reinforced polyetheretherketone, in *Mechanical Behavior of Biological and Biomimetic Materials,* edited by A.J. Bushby, V.L. Ferguson, C-C. Ko, and M.L. Oyen (Mater. Res. Soc. Symp. Proc. **898E**, Warrendale, PA, 2005), pp. L05–07.
43. J.Y. Rho, L. Kuhn-Spearing, and P. Zioupos: Mechanical properties and the hierarchical structure of bone. *Med. Eng. Phys.* **20,** 92 (1998).
44. J.D. Currey: Strength of bone. *Nature* **195,** 513 (1962).
45. J.D. Currey: The relationship between the stiffness and the mineral content of bone. *J. Biomech.* **2,** 477 (1969).
46. W. Voigt: *Lehrbuch der Kristallphysik*. (B.G. Teubner Verlag, Leipzig, Germany, 1928).
47. A. Reuss: Computation of the yield point of mixed crystals due to the plasticity condition for single crystals. *Z. Angew. Math. Mech.* **9,** 49 (1929).
48. Z. Hashin and S. Shtrikman: A variational approach to the theory of the elastic behaviour of multiphase materials. *J. Mech. Phys. Solids* **11,** 127 (1963).
49. J.L. Katz: Hard tissue as a composite material—I. Bounds on the elastic behaviour. *J. Biomech.* **4,** 455 (1971).
50. R. Hill: The elastic behaviour of a crystalline aggregate. *Proc. Phys. Soc.* **A65**, 351 (1952).
51. K. Piekarski: Analysis of bone as a composite material. *Int. J. Eng. Sci.* **11,** 557 (1973).
52. H.D. Wagner and S. Weiner: On the relationship between the microstructure of bone and its mechanical stiffness. *J. Biomech.* **25,** 1311 (1992).
53. U. Akiva, H.D. Wagner, and S. Weiner: Modelling the three-dimensional elastic constants of parallel-fibred and lamellar bone. *J. Mater. Sci.* **33,** 1497 (1998).
54. S. Weiner, W. Traub, and H.D. Wagner: Lamellar bone: Structure-function relations. *J. Struct. Biol.* **126,** 241 (1999).
55. J.C. Halpin: *Primer on Composite Materials Analysis* (Technomic Publishing Co., Lancaster, PA, 1992).

56. R. Hill: Theory of mechanical properties of fibre-strengthened materials: III. Self consistent model. *J. Mech. Phys. Solids* **13,** 189 (1965).
57. K.J. Bundy: *Experimental Studies of the Non-uniformity and Anisotropy of Human Compact Bone* (Stanford University, Palo Alto, CA, 1974).
58. K.J. Bundy: Determination of mineral-organic bonding effectiveness in bone—Theoretical considerations. *Ann. Biomed. Eng.* **13,** 119 (1985).
59. N. Sasaki, N. Ikawa, and A. Fukuda: Orientation of mineral in bovine bone and the anisotropic mechanical properties of plexiform bone. *J. Biomech.* **24,** 57 (1991).
60. H.J. Bunge: Effective elastic constants of cubic materials with arbitrary texture. *Kristall Techn.* **3,** 431 (1968).
61. H.J. Bunge, R. Kiewel, Th. Reinert, and L. Fritsche: Elastic properties of polycrystals—Influence of texture and stereology. *J. Mech. Phys. Solids* **48,** 29 (2000).
62. J.C. Halpin and N.J. Pagano: The laminate approximation for randomly oriented fibrous composites. *J. Comp. Mater.* **3,** 720 (1969).
63. C.W. Camacho, C.L. Tucker III, S. Yalvaç, and R.L. McGee: Stiffness and thermal expansion predictions for hybrid short fiber composites. *Polym. Compos.* **11,** 229 (1990).
64. P.J. Hine, R.A. Duckett, and I.M. Ward: Modelling the elastic properties of fibre-reinforced composites: II Theoretical predictions. *Compos. Sci. Technol.* **49,** 13 (1993).
65. H.R. Lusti, P.J. Hine, and A.A. Gusev: Direct numerical predictions for the elastic and thermoelastic properties of short fibre composites. *Compos. Sci. Technol.* **62,** 1927 (2002).
66. P.J. Hine, H.R. Lusti, and A.A. Gusev: Numerical simulation of the effects of volume fraction, aspect ratio and fibre length distribution on the elastic and thermoelastic properties of short fibre composites. *Compos. Sci. Technol.* **62,** 1445 (2002).
67. C.D. Price, P.J. Hine, B. Whiteside, A.M. Cunha, and I.M. Ward: Modelling the elastic and thermoelastic properties of short fibre composites with anisotropic phases. *Compos. Sci. Technol.* **66,** 69 (2006).
68. R.K. Roeder, G.L. Converse, H. Leng, and W. Yue: Kinetic effects on hydroxyapatite whiskers synthesized by the chelate decomposition method. *J. Am. Ceram. Soc.* **89,** 2096 (2006).
69. ASTM Standard D 638-01, *Standard Test Method for Tensile Properties of Plastics.* (American Society for Testing and Materials, West Conshohocken, PA, 2001).
70. J.B. Park: *Biomaterials: An Introduction*. (Plenum Press, New York, 1979).
71. J.L. Katz and K. Ukraincik: On the anisotropic elastic properties of hydroxyapatite. *J. Biomech.* **4,** 221 (1971).